Macromolecules

ARTICLE

pubs.acs.org/Macromolecules

Effect of Thickness on the Thermo-Mechanical Response of Free-Standing Thermoset Nanofilms from Molecular Dynamics

Chunyu Li and Alejandro Strachan*

School of Materials Engineering and Birck Nanotechnology Center, Purdue University, West Lafayette, Indiana 47906, United States

Supporting Information

ABSTRACT: We characterize how film thickness affects the thermo-mechanical response of free-standing nanofilms composed of a thermoset polymer, diglycidyl ether of Bisphenol A (DGEBA) with 3,3′-diaminodiphenyl sulfone (33DDS), via molecular dynamics. We find that the glass transition temperature, Young's modulus, and yield stress of the films decrease with decreasing thickness with the later two properties deviating from their bulk values at slightly larger thicknesses. The relative role of (i) intrinsic size effects, (ii) changes in quench depth ($T - T_g$), and (iii) variability in curing degree, on the depression of mechanical response of ultrathin films, are quantified. We find that intrinsic size effects contribute over 60% of the total change in mechanical response for the entire range of thicknesses studied.

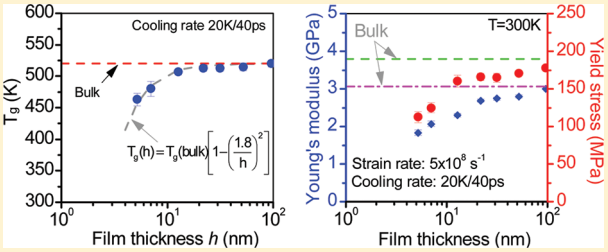

1. INTRODUCTION

Free-standing polymer nanofilms, with a macroscopic area but a thickness in the order of few tens or hundreds of nanometers, have many important applications in chemical sensors,[1] nano-mechanical sensors and actuators,[2,3] chemical separation,[4] tissue engineering,[5,6] and electronics.[7] Novel fabrication techniques have enabled nanoscale (thicknesses below 100 nm) free-standing polymer membranes in the past decade.[8−11] Although extending a nanometer structure laterally to millimeter or centimeter sizes remains a major challenge,[12] the potential applications of polymer nanofilms in numerous areas have stimulated great research interests in characterizing their physical properties and investigating surface and size effects. Understanding the surface and size effects is also important for polymers used in numerous traditional industries. For example, in polymer-based composite materials it is not uncommon to find very thin polymer regions separating or covering reinforcing fibers or particles.[13] Most of the work to date has focused on thermoplastic polymers and little is known about size effects in thermosets, despite their technological importance. In this paper we conduct molecular dynamics (MD) simulations to characterize the thermo-mechanical response of thermoset thin films consisting of epoxy resin diglycidyl ether of Bisphenol A (DGEBA) and cross-linking agent 3,3′-diaminodiphenyl sulfone (33DDS).

The glass transition temperature (T_g) is perhaps the best-characterized property in polymer nanofilms and a fundamental understanding of this phenomenon is critical since several others physical properties of amorphous polymers are associated with this transition point. The current state-of-the-art on the T_g of polymer films is reviewed by Alcoutlabi and McKenna in ref14. Although disagreements persist among different experimental methods, the general conclusion is that a free surface tends to reduce the T_g of an ultrathin polymer film with thickness below approximately 80 nm and the magnitude of reduction and the critical thickness depends on chemistry and molecular weight.[15,16] An empirical relation between film and bulk T_g proposed for polystyrene (PS) films[17] has been supported by other studies.[18] However, the relationship between changes in T_g with size, especially for thermosets, have not been fully established.

To fully realize the potential applications of polymer nanofilms, an in-depth understanding of their mechanical properties is also needed; however, few studies have addressed this topic because of the difficulties in nanoscale measurements. Stafford et al.[19] investigated the elastic moduli of ultrathin PS and poly(methyl methacrylate) (PMMA) films (with thickness from 5 to 200 nm) using a buckling-based metrology. The modulus was found to decrease from the bulk value when the thickness was reduced below 40 nm. Torres et al.[20,21] measured the elastic modulus of a series of PS and PMMA wrinkled films on an elastic substrate at ambient temperature using atomic force microscopy (AFM) and optical microscopy. They found that the elastic modulus also decreases in comparison to the bulk value as film thickness decreasing below a critical threshold. These studies indicate a critical film thickness for mechanical response below 100 nm for various systems. To our knowledge, the yield behavior of polymer nanofilms has not been characterized. The interplay between size effects on T_g and mechanical response is critical to develop a fundamental understanding of the response of nanoscale polymer films.

Although molecular modeling on polymers has become an indispensible tool for characterizing polymers alongside experiments,

Received: August 23, 2011
Revised: November 2, 2011
Published: November 16, 2011

ACS Publications © 2011 American Chemical Society

the overwhelming majority of these studies have concentrated on thermoplastics.[22−24] Among them, a few have studied free-standing polymer films and mostly concentrated on the glass transition temperature.[25−28] The prediction based on MD simulations that the glass transition temperature decreases with film thickness is consistent with experimental results. Yoshimoto et al.[29] used a coarse-grained polymer model to calculate local dynamic mechanical properties of free-standing thermoplastic thin films and found that overall stiffness of glassy thin films decreases with film thickness. Thermoset thin films remain vastly uncharacterized.

The objective of this paper is to understand the thermo-mechanical response of free-standing nanofilms of thermoset polymers. We employ a procedure previously developed by the authors to build molecular structure of DGEBA/33DDS thermoset films that combines MD simulations with a distance-based chemistry model.[30] The thermo-mechanical properties of the resulting structures are obtained via MD using the open source code LAMMPS[31] and the general-purpose Dreiding force field.[32] An alternative to all-atom simulations is coarse grain modeling where groups of atoms are lumped together into mesoparticles. These methods are computationally less intensive than all-atom MD due to the reduction in degrees of freedom and also because longer time scales can be used to integrate the equations of motion; consequently, they enable simulations of larger systems for longer times. However, while there have been significant advances in coarse-grain potentials[33−35] we are not aware of generally applicable parametrizations for thermoset polymers that provide the level of predictive power of all-atom simulations.

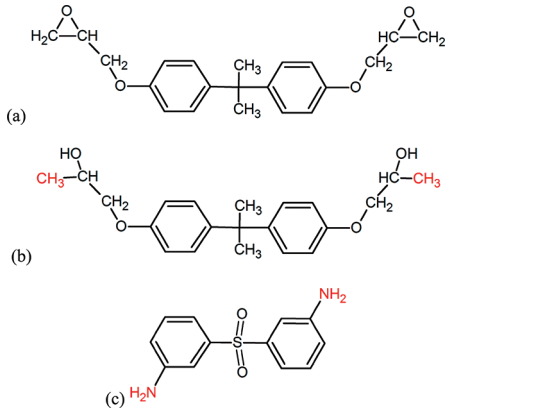

Figure 1. Molecular structures of (a) DGEBA, (b) activated DGEBA, and (c) 33DDS.

2. DGEBA/33DDS SYSTEMS AND MOLECULAR FORCE FIELD

2.1. Model System. Figure 1 shows the molecular structures of DGEBA and 33DDS. Our cross-linking procedure starts with the "activated" DGEBA molecule shown in Figure 1b. The reactive sites are highlighted in red. A small model system consisting of 16 monomers of DGEBA and 8 monomers of 33DDS, denoted (16, 8), is packed into a simulation cell using the MAPS software.[36] With an amine/epoxy molecular ratio equal to 1/2, a 100% conversion can be, in principle, reached. The small system is initially energy-minimized using conjugate gradients method and then equilibrated using an isothermal and isochoric (NVT ensemble) MD simulation for 50 ps. The simulation cells used for this study are obtained by replication of this small (16, 8) system followed by additional thermalization. The replication depends on the desired film thickness which ranges from 5 to 95 nm with a total number of atoms in the initial models from 17 000 to the largest 691 200, as listed in Table 1.

The initial model was packed at 600 K but at a low density 0.5 g/cm^3 and an isothermal, isobaric (*NPT*) simulation with pressure of 1 atm was conducted for 400 ps to take the system to its equilibrium atmospheric density, which is about 0.8 g/cm^3. The bulk models were then converted into films with free surfaces normal to the *z*-direction by increasing the cell length along *z* to create a vacuum separating periodic images of the films. Periodic boundary conditions are maintained in all three dimensions. After the liquid film is created it is further equilibrated by 100 ps of *NPT* simulations using a Nose−Hoover barostat that maintains the pressure at 1 atm and the ratios between the three cell dimensions constant, which prevents the periodic simulation cells from collapsing in the *z* direction and forming a bulk sample. The simulation times are enough for the liquid samples to achieve equilibrium; this is ensured by monitoring the time evolution of total energy and volume.

2.2. Force Field. The general-purpose Dreiding force field with harmonic covalent potential functions is employed in all our simulations. As was done previously, we use Lennard-Jones (LJ 6−12) functions to describe van der Waals interactions during the cross-linking process and Buckingham (exponential-6) during the calculation of the thermo-mechanical properties of the films. The Dreiding paper[32] describes an initial parametrization denoted Dreiding/A; we use the final, optimized parameters. Partial charges on DGEBA/33DDS, are obtained from self-consistent calculations using the electronegativity equalization method described in ref 30. The choice of interatomic potential is motivated from the fact that despite its simplicity, wide range of applicability and relatively small number of parameters, Dreiding with electronegativity equalization charges provide a

Table 1. Details of the Computational Samples

film	Mmonomers (DGEBA, 33DDS)	initial atoms	PBC cell size (nm^3)	film thickness at 300 K (nm)	cross-linking time (ns)	conversion degree (%)
F1	(256, 128)	17 280	10 × 10 × 20	5.18	3.50	81.25
F2	(512, 256)	34 560	10 × 10 × 20	6.98	3.55	83.89
F3	(1024, 512)	69 120	10 × 10 × 25	12.73	3.90	85.06
F4	(2048, 1024)	138 240	10 × 10 × 35	21.86	2.05	85.01
F5	(3072, 1536)	207 360	10 × 10 × 45	31.43	1.25	85.60
F6	(5120, 2560)	345 600	10 × 10 × 65	52.00	0.45	89.79
F7	(10240, 5120)	691 200	10 × 10 × 115	95.53	1.25	84.01

dx.doi.org/10.1021/ma201927n |*Macromolecules* 2011, 44, 9448–9454

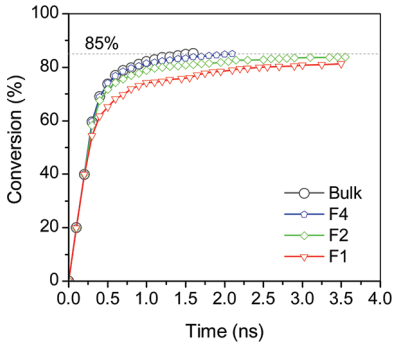

Figure 2. Conversion degree as a function of simulation time during MD simulations for bulk and various films.

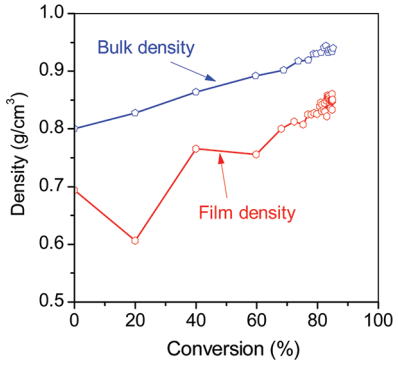

Figure 3. Mass density changes during curing for the film F3 (1024, 512) system (T = 600 K).

very accurate description of amorphous polymers. In particular, it provides an accurate description of elastic properties and glass transition temperature and the role of cross-linking degree in epoxy-based thermosets[30] and thermoplastics.[37] We include electronic versions of the LAMMPS input files for film F1 in the Supporting Information.[38]

3. CROSS-LINKING PROCEDURE

We use our recently developed MD-based polymerization simulator (MDPoS) to simulate the curing process of thermosets.[30] This method uses MD to describe the dynamics of the system and periodically check for nearby reactive atoms; new bonds are created between reactive atoms within a capture radius and a multigroup, multistep relaxation procedure is used to turn on new bonds smoothly. We run the procedure at T = 600 K, higher than experimentally, since we found that the increased mobility decreases network strain. The degree of conversion is defined as the ratio between the number of new bonds created and the maximum possible number of bonds between reactive carbon and nitrogen atoms. The conversion procedure is stopped when the conversion degree exceeds 85% or when the simulation time reaches a limit of 4 ns; as will be described below this leads to conversion degrees varying from 81.25 to 89.89% for the various films and bulk systems.

During simulations of the curing process, the conversion increases very quickly in the early stage but then slows down while the network grows continuously. All the seven model systems reached over 80% conversion. Figure 2 shows the

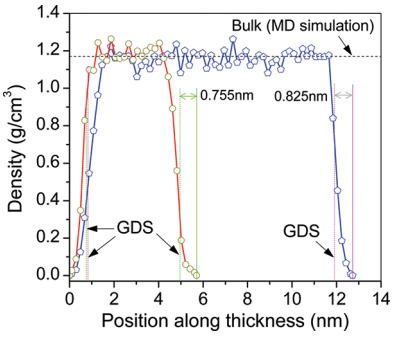

Figure 4. Density profiles across the film thickness for films F1 and F3 (T = 300 K).

evolution of conversion degree as a function of time; interestingly, thin films, with a larger fraction of undercoordinated surface molecules, exhibit slower reaction rates. Limited by the maximum simulation time (~4 ns), final films with different thicknesses have slightly different conversion degrees from 81.25% to 89.89%. This will be taken into account in the comparison of film properties.

The curing process can be further monitored following the change of total energy or density. Figure 3 shows the changes of average mass density as a function of conversion degree for film F3 (thickness 12.73 nm). As expected, the density increases with increasing conversion degree. Interestingly, we find a density increase of 20% for the F3 film system, much higher than the approximately 14% for (1024, 512) bulk system.

4. DENSITY PROFILE AND SURFACE ENERGY

Before cooling down, the cross-linked systems are equilibrated at 600 K for 200 ps using *NPT* simulations. The equilibrated structures are then cooled down to 300 K using *NPT* simulations where the ratio between cell dimensions are kept constant to avoid the collapse of the simulation cell dimension in the direction normal to the film surface. The cooling is performed in steps of 20 K running 40 ps at each temperature. Cooling rate has a significant effect on structural relaxations and T_g; consequently, rate effects should be accounted for when comparing results corresponding to different rates, for example when MD results are contrasted with experiments.[30,39] In our case, all films and bulk are cooled down with the same rate and, thus, size effects can be compared directly.

4.1. Density Profile. In order to calculate density profiles of the films we divide them into bins of roughly 2 Å width along their thickness and compute the total mass inside each bin based on atomic coordinates. Two typical density profiles are shown in Figure 4. We see that the average density in the interior of the films recovers almost exactly the bulk density (~1.17 g/cm^3 from our MD simulation and slightly less than the experimental value ~1.23 g/cm^3) regardless of film thickness. In the surface layers in both sides of a film, the density decreases to nearly zero. The thickness of the surface layer is less than 1.5 nm if counted from where the density begins to drop from its average values and does not depend on film thickness. This value is consistent with previous studies on thermoplastics.[27,40,41]

On the basis of the method of Gibbs dividing surface (GDS),[25] we also calculated the effective film thickness h_{eff}, defined as the distance between the left and the right GDS positions. The average density of a film is obtained by taking the mean value of

mass densities of 1/3 bins located at the central part of the film. The interfacial thickness is then obtained by $(h_{max} - h_{eff})/2$, where h_{max} stands for maximum film thickness. The calculated interfacial thickness is approximately 0.75−0.85 nm at the room temperature and in excellent agreement with previous predictions for thermoplastics.[41] This result indicates that thermosets and thermoplastics thin films exhibit very similar interfacial thickness. Temperature has a weak influence on interfacial thickness, see Figure 5. While our simulations exhibit large fluctuations intrinsic to the size of MD simulations, it is interesting to note that fluctuations in interfacial thickness increase for high temperatures. We see a noticeable increase at a temperature just below the overall T_g of the film, Figure 5; this observation may be related to the glass transition temperature of the surface layer being lower than that of the entire film.[42]

4.2. Surface Energy. A fundamental property of free-standing nanofilms is the surface energy (SE). For amine-cured epoxies, similar to our systems, experimental values of SE have been reported between 41 and 47 mJ/m^2.[43] We calculate the SE using the standard expression $(U_{film} - U_{bulk})/2A$, where the U_{film} is the potential energy of a film, U_{bulk} is the corresponding energy of a bulk sample and A is the area per free surface of the film (two free surfaces for a free-standing film).

Table 2 lists the total SE and the contributions from bonded and nonbonded components of the Dreiding force field computed for the film F3 (12.73 nm in thickness). The standard errors in the SE calculations were obtained by propagating standard deviations in the individual MD results, i.e., $\sigma_{SE}^2 = \sigma_{film}^2 + \sigma_{bulk}^2$. The total SE of 30 ± 15 mJ/m^2 is in good agreement with the experimental value for amine-cured epoxies. We find the dominant term in the SE to be van der Waals interactions. The energy contributions from the changes in bond angles, bond torsions and electrostatic interactions are of similar magnitude though different in contributing positively or negatively. Interestingly, angle and torsion energies in the thin films are lower than in the bulk; this is due to relaxation of network strain near the free surfaces.

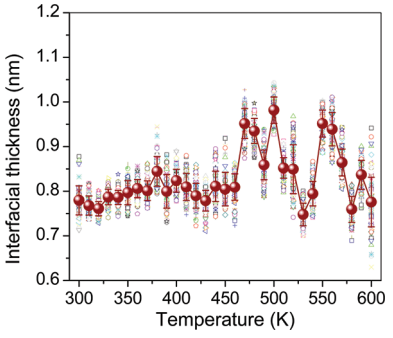

Figure 5. Interfacial thickness for a system (F3) as a function of temperature (the corresponding T_g = 507 K; open symbols represent individual thickness data corresponding to different times at the same temperature; filled symbols are averaged thickness).

5. GLASS TRANSITION TEMPERATURE

The glass transition temperature (T_g) for nanofilms can be determined from the density changes during cooling down of systems. Figure 6 shows the average density as a function of temperature for two films: one is very thin and another is relatively thick. A general trend of density increasing with decreasing temperature can be observed and the change in slope of the curves denotes T_g. Despite the larger fluctuation for very thin films, the slope change can be accurately determined by linear fits to the data for the low and high temperature regimes. The actual number of T_g and associated error estimates are obtained from the density−temperature data using segmented regression (R^2 > 0.998 with p value <0.0001 for F_test).[39]

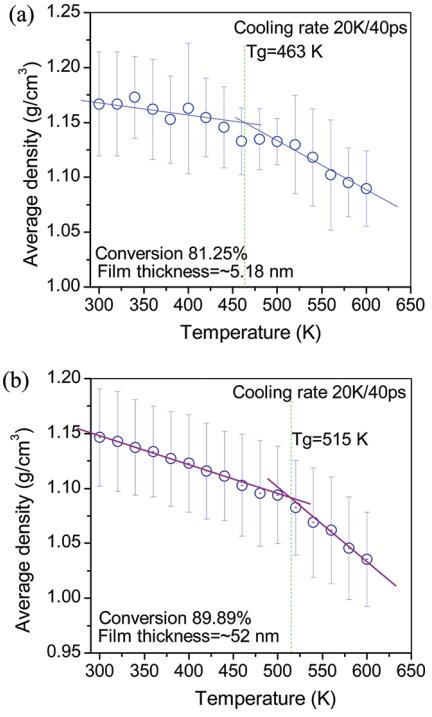

Figure 6. Determination of glass transition temperature for nanofilms: (a) film F1; (b) film F6.

Table 2. Calculation of Surface Energy

energy	E_{film} (kcal/mol)	E_{bulk} (kcal/mol)	$E_{film} - E_{bulk}$ (kcal/mol)	surface energy (mJ/m^2)[a]
bond	27896 (±153)	27824 (±136)	72 (±205)	4 (±12)
angle	38963 (±105)	39114 (±135)	−151 (±171)	−9 (±10)
dihedral	15394 (±49)	15570 (±84)	−176 (±97)	−10 (±6)
improper	1832 (±20)	1849 (±20)	−17 (±28)	−1 (±2)
van der Waals	22183 (±102)	21521 (±119)	662 (±157)	38 (±9)
coulomb	−58558 (±170)	−58688 (±190)	130 (±255)	8 (±15)
total	**47710 (±170)**	**47190 (±199)**	**520 (±262)**	**30 (±15)**[b]

[a] Surface area: A = 59.84 nm^2 [b] Surface energy for amine-cured epoxy by experiments: 41−47 mJ/m^2.[43]

dx.doi.org/10.1021/ma201927n |Macromolecules 2011, 44, 9448–9454

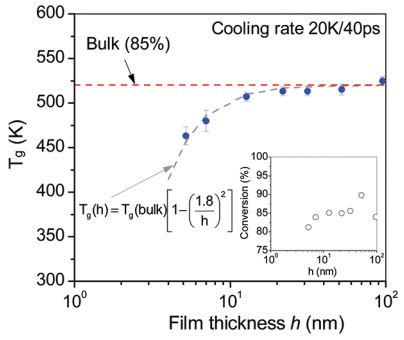

Figure 7. Glass transition temperature versus film thickness.

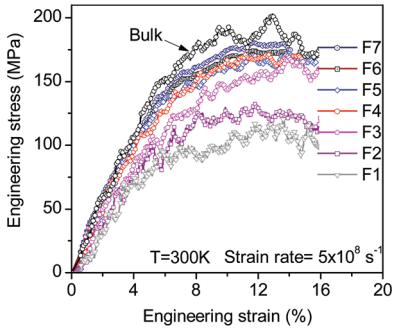

Figure 8. Stress−strain curves for films under in-plane uniaxial tension.

Figure 7 displays the variation of T_g as a function of film thickness h. T_g gradually decreases as the film thickness decreases. The maximum T_g depression for the thinnest film in this study is about 60K from the bulk value. Experimental works on PS films have led to an empirical relation for T_g as a function of film thickness (h): $T_g(h) = T_g(\text{bulk})[1 - (a/h)^{\delta}]$ with parameters $a = 3.2$ nm and $\delta = 1.8$ for PS.[17,18] We find that this function captures our MD data for DGEBA/33DDS thermosetting films accurately with $a = 1.8$ nm and $\delta = 2.0$. The fitting curve is shown as a dashed line in Figure 8.

Note the T_g shown above can only be understood as an averaged property for a film because it is based on the averaged density of the film. There is evidence that the T_g in the surface layers around the GDS positions would be much lower as suggested by previous studies of a two-layer model.[42] The lower T_g at the surface layers may be counted as the main reason for the T_g depression for the overall film. However, in thermoset polymers there is also another contributing factor for T_g depression in ultrathin thermoset films: changes in conversion degree. Figure 2 shows that conversion becomes much slower for ultrathin films. So the thinner films are very likely to have a lower conversion degree than the thicker film. Our previous studies[30,39] on bulk polymers have concluded that a 5% variation in conversion degree leads to a change of approximately 10−15 K on T_g. The inset in Figure 7 shows the conversion degree for films with different thickness. Thus, we estimate that 20% depression can be attributed to the lower conversion.

6. YOUNG'S MODULUS AND YIELD STRESS

The mechanical properties of nanofilms are important for most applications. We obtain the Young's modulus and yield stress for the film structures via nonequilibrium MD simulations. The films are uniaxially stretched along one of their periodic directions and a stress of 1 atm is maintained in the transverse direction. The cell dimension normal to the film surface is kept fixed at the initial value chosen to minimize electrostatic interactions between periodic images of the films. Because of this large fixed size in the dimension normal to film surfaces, the stress computed using the virial theorem by the MD simulation code (LAMMPS in our case) is not the actual stress and needs to be corrected by multiplying with the ratio of the fixed dimension to the actual film thickness. Stress−strain curves, as shown in Figure 8, are obtained under a strain rate of 5×10^8 s^{-1}. While this rate is high compared to what is used in experiments (other than shock loading) it is standard in MD simulations.

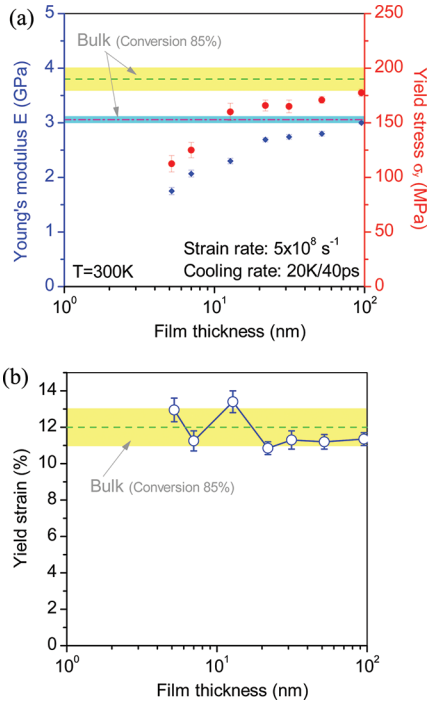

Figure 9. Mechanical properties versus film thickness: (a) Young's modulus and yield stress; (b) yield strain (colored shadows indicate error estimates for the bulk polymer).

We obtain Young's modulus by linearly fitting the MD raw data up to 4% strain (the error estimate in the figures is from the fitting). The yield stress is taken as the average between the maximum stress peak and its nearest local minimum (the error bar represents the difference between these two values) from the stress−strain curve, which is for the stress and strain after 100-points rolling average over the MD raw data. Figure 9a shows the Young's modulus and yield stress at $T = 300$ K for films with different film thickness. It is clear that both Young's modulus and yield stress decrease with film thickness relative to the bulk values. We calculate the yield strain corresponding to the yield stress defined above and its dependence with film thickness is depicted in Figure 9b. We find that while yield stress shows a clear size dependence, all the yield strain values lie within the range 10−14% (error bar indicates the difference of maximum and minimum). These values are also very close to the yield strain of bulk samples indicating that yield strain is very insensitive to film thickness.

Three factors can contribute to this reduction of film mechanical response with decreasing size. First, the conversion degree

dx.doi.org/10.1021/ma201927n |Macromolecules 2011, 44, 9448–9454

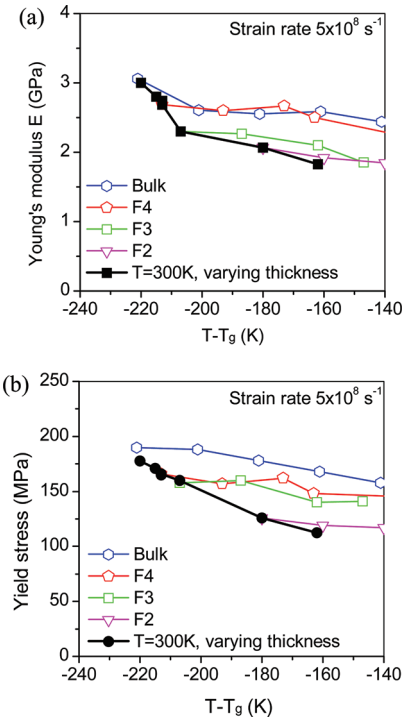

Figure 10. Effect of quench depth on mechanical properties (open symbols, films and bulk tested at various temperatures; full symbols, films of different thicknesses tested at T = 300 K).

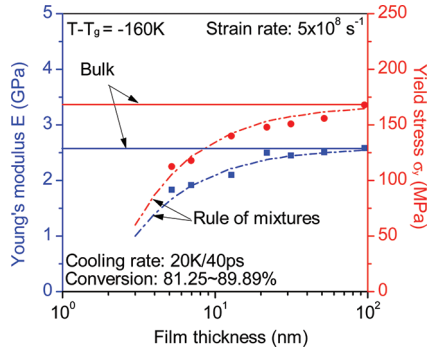

Figure 11. Mechanical properties versus film thickness at the same quench depth $T - T_g = -160$ K.

is slightly different for films with different thickness, as mentioned above. Previous MD simulations on a similar thermoset system[39] quantified the increase in Young modulus and yield stress with conversion degree. In the present case, the maximum deviation in film and bulk conversion is ±5%. Our prior results indicate this conversion factor contributes no more than 10% to the reduction of film mechanical properties.[39] The second and third factors are associated with size effects on T_g and intrinsic mechanical properties. The ultrathin films have T_g lower than the bulk system. Thus, room temperature mechanical properties represent different degrees of quench depths (T - T_g) for different polymer thicknesses with the consequent effect on mechanical response. Thinner film samples with smaller quench depths would be expected to exhibit depressed moduli and strength. These effects are extremely difficult to separate experimentally.[20] To test this effect we carried out mechanical deformation simulations for the various films at different testing temperatures, to vary the quench depth independently of film thickness. Parts a and b of Figure 10 show the Young's modulus and yield stress, respectively, as a function of $T - T_g$ for various films tested at different temperatures (the testing temperature can be recaptured by adding $T - T_g$ with T_g for a specific film given in Figure 7). The black lines with full symbols show the data obtained at room temperature but for different film thicknesses; the other curves correspond given thicknesses tested at various temperatures. Figure 10 separates the contribution to quench depth (open symbols) and intrinsic size effects on mechanical properties for a constant quench depth. We find a decrease in Young's modulus of approximately 0.7 GPa from bulk to a 7 nm film when compared at equivalent quench depths. Interestingly this stiffness depression is relatively insensitive to quench depth since the various samples exhibit similar softening with temperature. Very similar trends are observed for the yield stress, Figure 10(b), with a rather significant reduction in strength of about 100 MPa. If we compare the properties at the same $T - T_g$, the temperature effect on the reduction of the film properties relative to bulk system is estimated within 10−30%. Larger effect is seen on thinner films because of their lower T_g.

The intrinsic size effects on mechanical response are shown Figure 11 where mechanical properties are shown versus film thickness at the same $T - T_g = -160$ K, i.e., excluding the quench depth effect. The remaining issue is the origin of this intrinsic size effect. In section 4.1 we have seen that the thickness of the surface layer is about 1.5 nm regardless of film thickness. The mass density in this surface layer is nonuniform and much lower than the density in the interior layer. The surface layer also has been predicted to have a much lower T_g. Thus, lower stiffness and strength are expected for the two surface layers. Simulations of Yoshimoto et al.[29] on local mechanical properties of thermoplastics provide a support to this expectation. If we describe the polymer nanofilm as a composite with a stiff and strong interior surrounded by two softer and weaker surface layers, the rule of mixtures for an isostrain condition can be used to model the reduction of film stiffness and strength. Assume that the surface layer with thickness $h_{surface}$ =1.5 nm has a average Young's modulus $E_{surface}$ =1.0 GPa and a yield stress $\sigma_{surface}$ =60 MPa, and the interior layer exhibits bulk properties, simple calculations based on the rule of mixtures ($E = E_{bulk}(1 - h_{surface}/h) + E_{surface}(h_{surface}/h)$, $\sigma = \sigma_{bulk}(1 - h_{surface}/h) + \sigma_{surface}(h_{surface}/h)$, in which h is the film thickness) result in the two dash lines in Figure 11, leading to very good agreement with the simulation data. Because of the roughly fixed thickness of the surface layer, the volume fraction of surface layers in thicker film is small compared with thinner films. Thus, the surface effect on thicker films is relative small. This explains why film properties approach to the bulk's when film thickness increases.

7. CONCLUSIONS

We have conducted MD simulations on free-standing thermoset polymer nanofilms. The curing simulations using MDPoS indicates that a significant slowdown of chemical reactions as the thickness of the films decrease and that ultrathin films may exhibit lower curing degrees than their bulk counterparts. The glass transition temperature is found to decrease with decreasing film thickness deviating from their bulk value at critical thickness in the range of 50−80 nm. Young's modulus and the yield stress are also found to decrease with decreasing film thickness but with

a slightly larger critical thickness of around or over 100 nm. Our simulations also show that the depression of mechanical properties in thin films is dominated by intrinsic size effects with the difference in quench depth and variations in cross-linking degree accounting for less than 40% of the change observed from the bulk to a 5 nm film.

■ ASSOCIATED CONTENT

Supporting Information. Dreiding and LAMMPS data files. This material is available free of charge via the Internet at http://pubs.acs.org.

■ ACKNOWLEDGMENT

This work was supported by a grant with The Boeing Company and the US National Science Foundation (NSF) under Contract CMMI-0826356. Computational resources on nanoHUB.org are gratefully acknowledged.

■ REFERENCES

(1) Arora, W. J.; Tenhaeff, W. E.; Gleason, K. K.; Brbastathis, G. *J. Microelectromech. Syst.* **2009**, *18*, 97–102.
(2) Kang, T. J.; Cha, M.; Jang, E. Y.; Shin, J.; Im, H. U.; Kim, Y.; Lee, J.; Kim, Y. H. *Adv. Mater.* **2008**, *20*, 3131–3137.
(3) Zeng, T.; Claus, R.; Zhang, F.; Du, W.; Cooper, K. L. *Smart Mater. Struct.* **2001**, *10* (4), 780–785.
(4) Uhlmann, P.; Varnik, F.; Truman, P.; Zikos, G.; Moulin, J. F.; Muller-Buschbaum, P.; Stamm, M. *J. Phys.-Condens. Matter* **2011**, *23*, 184123.
(5) Tang, Z.; Wang, Y.; Podsiadlo, P.; Kotov, N. A. *Adv. Mater.* **2006**, *18*, 3203–3224.
(6) Fujie, T.; Matsutani, N.; Kinoshita, M.; Okamura, Y.; Saito, A.; Takeoka, S. *Adv. Funct. Mater.* **2009**, *19*, 2560–2568.
(7) Horowitz, G. *J. Mater. Res.* **2004**, *19*, 1946–1962.
(8) Ono, S. S.; Decher, G. *Nano Lett.* **2006**, *6*, 592–598.
(9) Jiang, C.; Markutsya, S.; Tsukruk, V. V. *Adv. Mater.* **2004**, *16*, 157–161.
(10) Mallwitz, F.; Goedel, W. A. *Angew. Chem., Int. Ed.* **2001**, *40*, 2645–2647.
(11) Mattsson, J.; Forrest, J. A.; Borjesson, L. *Phys. Rev. E* **2000**, *62*, 5187–5200.
(12) Vendamme, R.; Ohzono, T.; Nakao, A.; Shimomura, M.; Kunitake, T. *Langmuir* **2007**, *23*, 2792–2799.
(13) Morgan, P. *Carbon Fibers And Their Composites*. CRC Press, Taylor & Francis Group: New York, 2005.
(14) Alcoutlabi, M.; McKenna, G. B. *J. Phys.: Condens. Matter* **2005**, *17*, R461–R524.
(15) Forrest, J. A.; Dalnoki-Veress, K.; Stevens, J. R.; Dutcher, J. R. *Phys. Rev. Lett.* **1996**, *77*, 2002–2005.
(16) Dalnoki-Veress, K.; Forrest, J. A.; Murray, C.; Gigault, C.; Dutcher, J. R. *Phys. Rev. E* **2001**, *63*, 031801.
(17) Keddie, J. L.; Jones, R. A. L.; Cory, R. A. *Europhys. Lett.* **1994**, *27*, 59–64.
(18) Forrest, J. A.; Dalnoki-Veress, K. *Adv. Colloid Interface Sci.* **2001**, *94*, 167–196.
(19) Stafford, C. M.; Vogt, B. D.; Harrison, C.; Julthongpiput, D.; Huang, R. *Macromolecules* **2006**, *39*, 5095–5099.
(20) Torres, J. M.; Stafford, C. M.; Vogt, B. D. *ACS Nano* **2009**, *3*, 2677–2685.
(21) Torres, J. M.; Stafford, C. M.; Vogt, B. D. *Polymer* **2010**, *51*, 4211–4217.
(22) Stachurski, Z. H. *Prog. Polym. Sci.* **1997**, *22*, 407–474.
(23) Baschnagel, J.; Varnik, F. *J. Phys.: Condens. Matter* **2005**, *17*, R851–R953.
(24) Rottler, J. *J. Phys.: Condens. Matter* **2009**, *21*, 463101.
(25) Peter, S.; Meyer, H.; Baschnagel, J. *J. Polym. Sci., B: Polym. Phys.* **2006**, *44*, 2951–2967.
(26) Alexiadis, O.; Khare, R.; Beckers, J.; Baljon, A. R. C.; Mavrantzas, V. G. *Macromolecules* **2008**, *41*, 987–996.
(27) Baljon, A. R. C.; Williams, S.; Balabaev, N. K.; Paans, F.; Hudzinskyy, D.; Lyulin, A. V. *J. Polym. Sci., B: Polym. Phys.* **2010**, *48*, 1160–1167.
(28) Kim, S.; Torkelson, J. M. *Macromolecules* **2011**, *44*, 4546–4553.
(29) Yoshimoto, K.; Jain, T. S.; Nealey, P. F.; de Pablo, J. J. *J. Chem. Phys.* **2005**, *122*, 144712.
(30) Li, C. Y.; Strachan, A. *Polymer* **2010**, *51*, 6058–6070.
(31) LAMMPS-Large-scale Atomic/Molecular Massively Parallel Simulator (release of August 16, 2009), http://lammps.sandia.gov .
(32) Mayo, S. L.; Olafson, B. D.; Goddard, W. A. *J. Phys. Chem.* **1990**, *94*, 8897–8909.
(33) Milano, G.; Muller-Plathe, F. *J. Phys. Chem. B* **2005**, *109*, 18609–18619.
(34) Fritz, D.; Harmandaris, V. A.; Kremer, K.; van der Vegt, N. F. A. *Macromolecules* **2009**, *42*, 7579–7588.
(35) Rossi, G.; Giannakopoulos, I.; Monticelli, L.; Rostedt, N. K. J.; Puisto, S. R.; Lowe, C.; et al. *Macromolecules* **2011**, *44*, 6198–6208.
(36) *MAPS-The Materials And Processes Simulations platform*; Scienomics Inc.: Stamford, CT, 2008.
(37) Jaramillo, E.; Wilson, N.; Christensen, S.; Gosse, J.; Strachan, A. *Phys. Rev. B* **2011**, to be published.
(38) Supporting Information includes LAMMPS input files for a thermoset film.
(39) Li, C. Y.; Strachan, A. *Polymer* **2011**, *52*, 2920–2928.
(40) Mistra, S.; Fleming, P. D.; Mattice, W. L. J. *Comput. Aided Mater. Des.* **1995**, *2*, 101–112.
(41) Mansfield, K. F.; Theodorou, D. N. *Macromolecules* **1991**, *24*, 6283–6294.
(42) DeMaggio, G. B.; Frieze, W. E.; Gidley, D. W.; Zhu, M.; Hristov, H. A.; Yee, A. F. *Phys. Rev. Lett.* **1997**, *74*, 4947–4950.
(43) Chen, D.; Pascault, J. P. *Makromol. Chem.* **1991**, *192*, 867–882.